J. Fluid Mech. (1986), *vol.* 171, *pp.* 495–508
Printed in Great Britain

Motion of a single capsule in a hydraulic pipeline

By Y. TOMITA, M. YAMAMOTO AND K. FUNATSU
Department of Mechanical Engineering, Kyushu Institute of Technology,
Tobata, Kitakyushu 804, Japan

(Received 3 March 1986)

The method of characteristics is used to numerically analyse the motion of a single solid capsule in a hydraulic horizontal straight pipe. The capsule is assumed to be a point mass and the coaxial-annular-flow model around the capsule is used to derive the boundary conditions for water flow at the capsule discontinuity. The results are compared with experimental measurements which were taken in a pipeline 28 m in length and with an inside diameter of 40 mm. The capsule had wheels to keep its position coaxial with the pipe axis and always had a higher velocity than the water flow. The measurements are explained quite well by the analysis.

1. Introduction

The capsule pipeline is a system which transports solids in capsules carried through a pipeline by a flowing fluid. The hydraulic capsule pipeline usually uses water as the carrier fluid and can easily carry heavy materials like ore. The capsule is suspended by water flow without contact with the wall in a horizontal pipeline even if the capsule is heavier than water. Thus a hydraulic capsule pipeline does not always require wheeled capsules. On the other hand, a pneumatic capsule pipeline requires wheeled capsules because air is lighter than water. However, Yokogawa *et al.* (1980) recommend wheeled capsules even in a hydraulic capsule pipeline in order to transport heavy materials in large quantities over a long distance with a steep slope.

Liu (1981) gives a detailed review of hydraulic capsule transport in general, and there are now many references available. Most of them, however, concern steady flow and very little is known about the unsteady motion of individual capsules in a pipeline or about transient water flow caused by the capsule motion. In this paper we pursue the motion of a single capsule in a horizontally straight pipeline from the feeding point to the pipe end. We assume that the capsules are cylindrical and that their posture in the pipe is always constant, and hence we exclude problems like 'lift off' peculiar to the non-wheeled capsules.

There is a well-known analysis of water hammer in a pipe based on the method of characteristics. The analysis is now fully established and is applicable to our research. Lur'e & Gol'dzberg (1971) propose a numerical analysis of pneumatic capsule transport which is based on the method of characteristics, and here we apply their method with a little modification. A capsule is moved by fluid forces, consisting of the pressure and shear forces, acting on its surface. However, if we use the drag coefficient, which is usually measured in a steady flow, to calculate the forces in the unsteady motion of the capsule, a complicated problem concerning unsteady forces arises caused by added mass, which is important in our research because the density differences between the fluid and the capsule is relatively small. This problem is avoided if we directly calculate the forces by integrating the pressure and shear stresses acting on the capsule surface. The forces are related to water flow around

the capsule, which is determined by the capsule geometry. A flow model that does not pass water through the clearance between the capsule and the pipe wall is one of the simplest. In this model the fluid forces turn out to be pressure force alone and the capsule velocity is necessarily equal to the water velocity. A model that calculates the clearance flow using the equation of orifice discharge is called an orifice flow model and is often used for the pneumatic capsule. In this model the capsule velocity is always smaller than the water velocity, because the direction of the water flow through the clearance is from the higher-pressure side to the lower, and the pressure at the rear of the capsule is usually higher than that at the front. In these models the capsule velocity cannot exceed the water velocity and, as is well known, this is not always the case for the hydraulic capsule. Therefore, it is necessary to devise a more elaborate model. In this paper we apply the coaxial-annular-flow model which was used by Yanaida (1980) and Polderman (1982) and take advantage of the experimental findings by Tsuji, Morikawa & Chono (1980). In addition, results are given from experiments on single-capsule motion in a horizontal pipeline with a constant head. These results are compared with the numerical analysis.

2. Theory

2.1. *Basic equations*

The equations for unsteady water flow in pipes are well known and are given by

$$\frac{1}{\rho a^2}\frac{\partial p}{\partial t}+\frac{\partial V}{\partial x}=0, \tag{1}$$

$$\frac{1}{\rho}\frac{\partial p}{\partial x}+\frac{\partial V}{\partial t}=-\lambda\frac{V|V|}{2D}, \tag{2}$$

where p represents pressure, V the area mean velocity, x the axial coordinate, t the time, D the pipe inside diameter, λ the pipe friction coefficient for water, ρ the density of water and a the propagating velocity of the water pressure wave. If κ is the volumetric modulus of elasticity of water, E the Young's modulus of pipe material and δ the thickness of the pipe wall, then a is given by

$$a=\left(\frac{\kappa/\rho}{1+(\kappa D/E\delta)}\right)^{\frac{1}{2}}. \tag{3}$$

The equation of motion for the capsule is given by

$$M\ddot{Z}=F-fg|M-\rho V_c|, \tag{4}$$

where M is the capsule mass, Z the capsule coordinate, F the fluid forces acting on the capsule in the axial direction, f the coefficient of the Coulomb friction, g the acceleration due to gravity and V_c the capsule volume. The Coulomb friction will have an effect, if the capsule is not neutrally suspended by water flow, in preventing contact with the pipe wall.

Here, we treat the capsule as a point mass when calculating water flow, but the velocity and the pressure are likely to change at the capsule discontinuously:

$$x=Z^-;\quad p=p_R,\quad V=V_R, \tag{5}$$

$$x=Z^+;\quad p=p_F,\quad V=V_F, \tag{6}$$

where we denote the value at the rear and front of the capsule by the subscripts R and F.

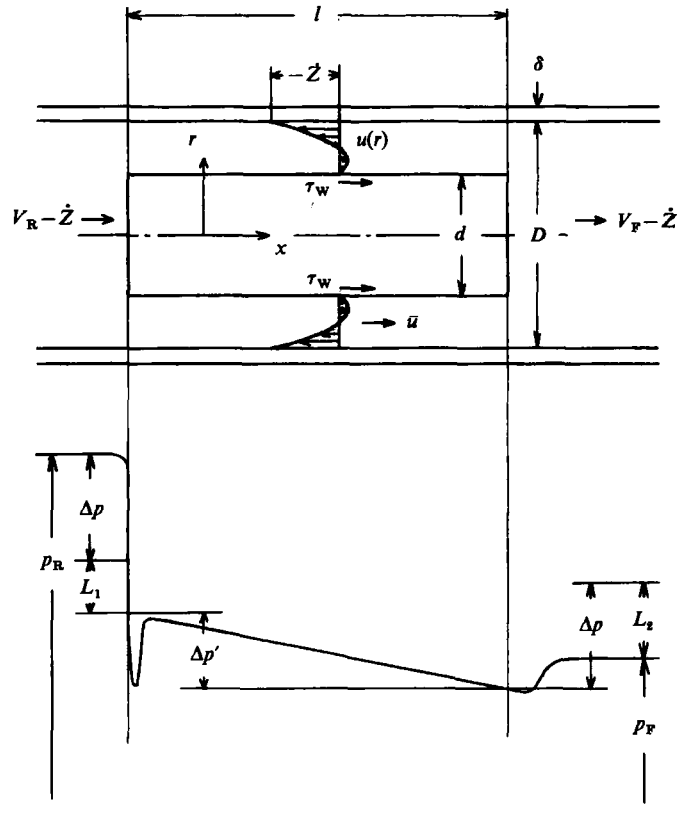

FIGURE 1. Coaxial-annular-flow model around a capsule.

2.2. *The coaxial-annular-flow model*

The fluid forces and the clearance flow should be given by the capsule velocity $\dot{Z}$ and V and p at both sides of the capsule. They are determined by the water flow around the capsule, which is influenced by the capsule geometry. We assume that the capsule is a cylinder of length l and diameter d, as shown in figure 1 and that it is suspended coaxially and has no spin. We apply a reference frame moving with the capsule. Then the relation between $\dot{Z}$ and water velocity is given by

$$V_{\mathrm{R}}-\dot{Z}=\left\{1-\left(\frac{d}{D}\right)^2\right\}\bar{u}, \tag{7}$$

$$V_{\mathrm{F}}-\dot{Z}=\left\{1-\left(\frac{d}{D}\right)^2\right\}\bar{u}, \tag{8}$$

where $\bar{u}$ is the area mean water velocity in the clearance, which is relative to the capsule velocity. From (7) and (8) we have

$$V_{\mathrm{R}}=V_{\mathrm{F}}. \tag{9}$$

Tsuji *et al.* (1980) measured the pressure distribution of air flow around the stationary capsule as shown in figure 1, which is schematically drawn based on their measurements. We illustrate a case where p_{R} is larger than p_{F} and $\bar{u}$ is positive. Δp is the idealized pressure drop due to abrupt contraction at the rear, which is calculated by

Bernoulli equation. L_1 is the pressure loss caused by abrupt contraction, L_2 is that due to abrupt enlargement at the front side, and $\Delta p'$ is the pressure drop in the clearance. Their research confirmed that L_1 is accurately estimated by the well-known Weisbach data and L_2 by the Borda–Carnot analysis. It also showed that the pressure at the rear is equal to the stagnation pressure $p_R+\frac{1}{2}\rho(V_R-\dot{Z})^2$ and that the pressure at the front is equal to the static pressure p_F. We can calculate the fluid forces by summing the pressure force F_p caused by the pressure difference between both ends and the shear force F_s due to the fluid friction acting on the cylindrical surface. Then, F_p is given by

$$F_p = \tfrac{1}{4}\pi d^2\{(p_R-p_F)+\tfrac{1}{2}\rho(V_R-\dot{Z})^2\}. \tag{10}$$

There are several models for evaluating the shear force. We assume that the clearance flow is a fully developed coaxial annular flow under a constant pressure gradient dp/dx in the clearance, and the velocity distribution in the clearance u is calculated as follows:

$$u = \frac{1}{4\mu}\frac{dp}{dx}\left\{r^2-\left(\frac{d}{D}\right)^2\right\}-\frac{\ln(2r/d)}{\ln(D/d)}\left\{\dot{Z}+\frac{1}{16\mu}\frac{dp}{dx}(D^2-d^2)\right\}, \tag{11}$$

where r the radial coordinate and μ the viscosity of water. Then, the shear force is given by

$$F_s = \pi d\int_0^l \mu\left.\frac{du}{dr}\right|_{r=\frac{1}{2}d} dx = \tfrac{1}{8}\pi D^2 l\frac{dp}{dx}\left(2k^2+\frac{1-k^2}{\ln k}\right)+\frac{2\pi\mu l\dot{Z}}{\ln k}, \tag{12}$$

where k is $(d/D)^2$. The pressure gradient dp/dx is approximated by $-\Delta p'/l$ and is accurately given by

$$\frac{dp}{dx} = -\frac{p_R-p_F}{l}+\frac{\zeta+k^4}{(1-k^2)^2 l}\tfrac{1}{2}\rho(V_R-\dot{Z})^2, \tag{13}$$

where ζ is the loss coefficient of abrupt contraction. Thus the fluid forces F are given by

$$\begin{aligned} F &= F_p+F_s \\ &= \tfrac{1}{8}\pi D^2\frac{1-k^2}{\ln k}(p_R-p_F)+\frac{2\pi\mu l Z}{\ln k}+\left\{\frac{1+\zeta}{(1-k^2)^2}+\frac{\zeta+k^4}{2k^2(1-k^2)\ln k}\right\}\tfrac{1}{8}\pi D^2k^2\rho(V_R-\dot{Z})^2. \end{aligned} \tag{14}$$

$\bar{u}$ can be derived from (11) and (13):

$$\begin{aligned} \bar{u} &= \frac{4}{\pi(D^2-d^2)}\int_{\frac{1}{2}d}^{\frac{1}{2}D} 2\pi r u\,dr \\ &= \frac{D^2}{32\mu l}\left(1+k^2+\frac{1-k^2}{\ln k}\right)\left\{(p_R-p_F)-\frac{\zeta+k^4}{(1-k^2)^2}\tfrac{1}{2}\rho(V_R-\dot{Z})^2\right\}-\left(\frac{1}{1-k^2}+\frac{1}{2\ln k}\right)\dot{Z}. \end{aligned} \tag{15}$$

Thus we get the required equations (14) and (15), which relate F and $\bar{u}$ to V_R, V_F, p_R, p_F and $\dot{Z}$.

When $\bar{u}$ is negative, (10) and (11) undergo small changes, and instead of (14) and (15) we have

$$F = -\tfrac{1}{8}\pi D^2\frac{1-k^2}{\ln k}(p_R-p_F)+\frac{2\pi\mu l\dot{Z}}{\ln k}-\left\{\frac{1+\zeta}{(1-k^2)^2}+\frac{\zeta+k^2}{2k^2(1-k^2)\ln k}\right\}\tfrac{1}{8}\pi D^2k^2\rho(V_F-\dot{Z})^2 \tag{16}$$

and

$$\bar{u} = \frac{D^2}{32\mu l}\left(1+k^2+\frac{1-k^2}{\ln k}\right)\left\{(p_R-p_F)+\frac{\zeta+k^2}{(1-k^2)^2}\tfrac{1}{2}\rho(V_F-\dot{Z})^2\right\}-\left(\frac{1}{1-k^2}+\frac{1}{2\ln k}\right)\dot{Z}. \tag{17}$$

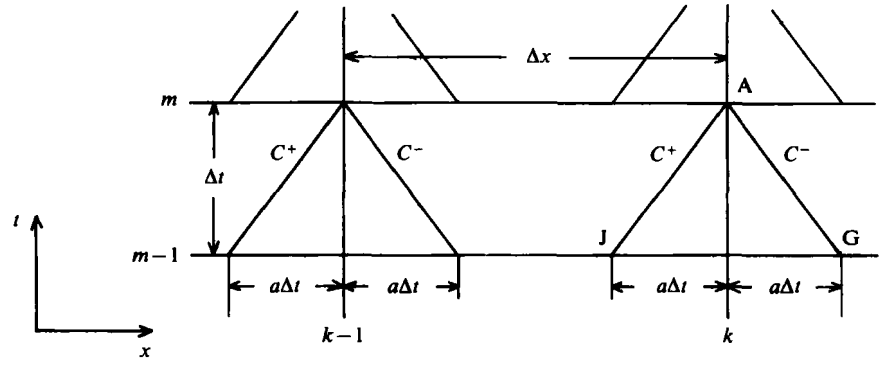

FIGURE 2. Grid system.

3. Method of computation

3.1. *Basic scheme*

Equations (1) and (2) are a hyperbolic system and are solved numerically by the method of characteristics. The grid system used for the computation is shown in figure 2. The values of p and V at grid points on $t = (m-1)\,\Delta t$ can be determined by the values on $t = (m-2)\,\Delta t$, where Δt is the timestep in the computation and m is the integer. For example, to determine the values at point A, we draw the forward and backward characteristics C^+ and C^- which pass point A. Points J and G are the intersecting points of the characteristics with the line $t = (m-2)\,\Delta t$. The values at J and G are given by the known values at the grid points on $t = (m-2)\,\Delta t$ by interpolation. Then we have the following relations along the C^+ and C^-:

$$H_{\mathrm{A}}^m - H_{\mathrm{J}}^{m-1} = -B(V_{\mathrm{A}}^m - V_{\mathrm{J}}^{m-1}) + R_{\mathrm{J}}^{m-1}, \tag{18}$$

$$H_{\mathrm{A}}^m - H_{\mathrm{G}}^{m-1} = -B(V_{\mathrm{A}}^m - V_{\mathrm{G}}^{m-1}) + R_{\mathrm{G}}^{m-1}, \tag{19}$$

where H is the pressure head defined as $p = \rho g(H - H_0)$, provided that H_0 is a reference head, B is a/g and R is the friction head given by

$$R = -\frac{\lambda V|V|}{2gD} a\Delta t. \tag{20}$$

The superscripts indicte the time and the subscripts the axial position. H_{A}^m and V_{A}^m are determined by (18) and (19). The explanation of this method can be easily found, for example, in Zucrow & Hoffman (1976).

3.2. *Capsule boundary*

Now we consider the case where the capsule trajectory crosses the characteristics, as shown in figure 3. In this example, the values at point A are influenced by the capsule trajectory. First we determine the values H_{R}^m, H_{F}^m, V_{R}^m and V_{F}^m at both ends of the capsule. Then we determine V_{k-1}^m and H_{k-1}^m by H_{k-2}^m, H_{R}^m, V_{k-2}^m and V_{R}^m. We have along both characteristics through Z^m

$$H_{\mathrm{R}}^m - H_{\mathrm{VP}}^{m-1} = -B(V_{\mathrm{R}}^m - V_{\mathrm{VP}}^{m-1} + R_{\mathrm{VP}}^{m-1}, \tag{21}$$

$$H_{\mathrm{F}}^m - H_{\mathrm{WP}}^{m-1} = B(V_{\mathrm{F}}^m - V_{\mathrm{WP}}^{m-1}) + R_{\mathrm{WP}}^{m-1}, \tag{22}$$

where H_{VP}^{m-1}, V_{VP}^{m-1} and R_{VP}^{m-1} are calculated from H_{k-1}^{m-1}, H_{k-2}^{m-1}, V_{k-1}^{m-1} and V_{k-2}^{m-1}, and H_{WP}^{m-1}, V_{WP}^{m-1} and R_{WP}^{m-1} are by H_{FB}^{m-1}, H_k^{m-1}, V_{FB}^{m-1} and V_k^{m-1}. Besides (9) we need one

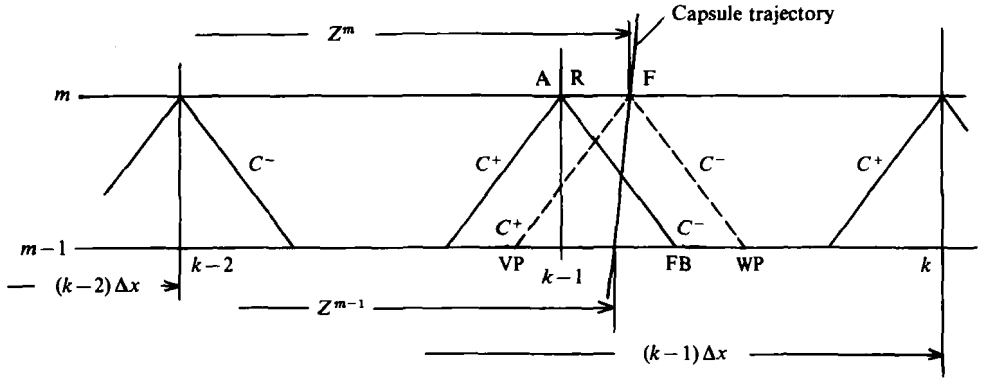

FIGURE 3. Influence of capsule trajectory.

more equation to determine the four unknowns. This equation depends on the flow model, but is obtained from (7) and (15) or (8) and (18) in the present model. If $\bar{u}$ is positive, we get the following equation from (7) and (15):

$$\alpha(V_R^m-\dot{Z}^{m-1})^2+(1+\beta B)(V_R^m-\dot{Z}^{m-1})-\{\beta\delta-2(\beta B+\gamma)\dot{Z}^{m-1}\}=0, \tag{23}$$

where

$$\alpha=\frac{\rho D^2}{32\mu l}\left(1+k^2+\frac{1-k^2}{\ln k}\right)\frac{\zeta+k^4}{1-k^2}, \tag{24}$$

$$\beta=\frac{\rho g D^2(1-k^2)}{16\mu l}\left(1+k^2+\frac{1-k^2}{\ln k}\right), \tag{25}$$

and

$$\gamma=1+\frac{1-k^2}{\ln k}. \tag{26}$$

By solving (23) we obtain

$$V_R^m=\dot{Z}^{m-1}+\frac{\beta\delta-2(\beta B+\gamma)\dot{Z}^{m-1}}{(1+\beta B)+[(1+\beta B)^2+\alpha\{\beta\delta-2(\beta B+\gamma)\dot{Z}^{m-1}\}]^{\frac{1}{2}}}, \tag{27}$$

where we choose a positive root, and next

$$\delta\geqslant 2\left(B+\frac{\gamma}{\beta}\right)\dot{Z}^{m-1} \tag{28}$$

is necessary because we assume $\bar{u}$ to be positive. When $\bar{u}$ is negative, we have from (8) and (18)

$$V_F^m=\dot{Z}^{m-1}+\frac{\beta\delta-2(\beta B+\gamma)\dot{Z}^{m-1}}{(1+\beta B)+[(1+\beta B)^2-\alpha\{\beta\delta-2(\beta B+\gamma)\dot{Z}^{m-1}\}]^{\frac{1}{2}}}, \tag{29}$$

and

$$\delta<2\left(B+\frac{\gamma}{\beta}\right)\dot{Z}^{m-1}. \tag{30}$$

Thus, we can determine H_R^m and H_F^m from (21) and (22), and H_A^m and V_A^m are given by the interpolation

$$H_{k-1}^m=H_{k-2}^m+\frac{(H_R^m-H_{k-2}^m)\Delta x}{Z^m-(k-2)\Delta x}, \tag{31}$$

$$V_{k-1}^m=V_{k-2}^m+\frac{(V_R^m-V_{k-2}^m)\Delta x}{Z^m-(k-2)\Delta x}, \tag{32}$$

where Δx is the step in the axial direction.

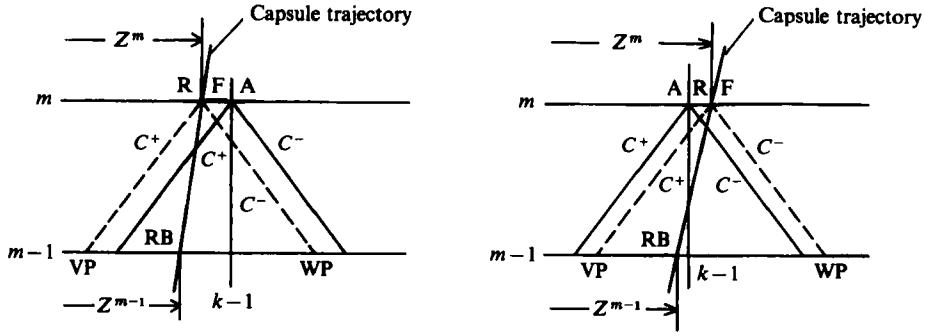

FIGURE 4. Influence of capsule trajectory.

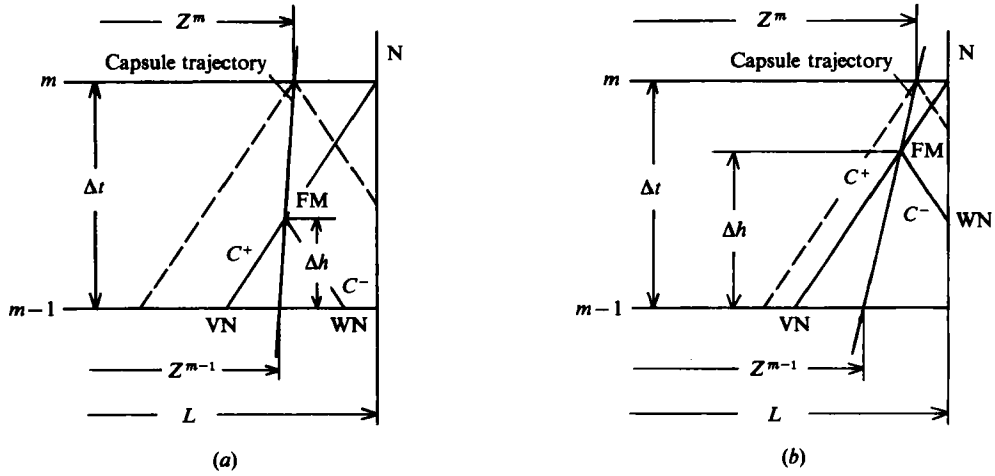

FIGURE 5. Capsule trajectory and exit boundary. (*a*) $\Delta h < \frac{1}{2}\Delta t$; (*b*) $\Delta h > \frac{1}{2}\Delta t$.

There are two other cases where the grid point A is influenced by the capsule trajectory, as shown in figure 4. In those cases the values of V and H are obtained in a similar manner to that described above.

3.3. *Fixed boundary*

In this computation the capsule is placed near the pipe inlet and the computation is stopped when the capsule leaves the pipe exit. The inlet and exit heads are kept constant. At the exit, however, special consideration is needed when the capsule trajectory crosses the characteristics C^+ which passes the last grid point, as shown in figure 5. We determine the values at point N and then those at the rear and front of the capsule. We define Δh as the time when the trajectory intersects C^+ which passes N. When Δh is smaller than $\frac{1}{2}\Delta t$, as shown in figure 5(*a*), from H_{VN}^{m-1}, H_{WN}^{m-1}, V_{VN}^{m-1} and V_{WN}^{m-1} we can determine H_{FM} and V_{FM}, which are the values at the front of the capsule at the intersction. WN is the intersection of the characteristics C^- and the line $t = (m-2)\,\Delta t$, and H_{WN}^{m-1} and V_{WN}^{m-1} are given by the interpolation. Since H_{N}^{m} is specified, then V_{N}^{m} is determined by H_{FM}, V_{FM} and H_{N}^{m}. When Δh is larger than $\frac{1}{2}\Delta t$, as shown in figure 5(*b*), the characteristics C^- which passes the intersection crosses the line $x = L$, where L is the length of the pipeline. We obtain H_{WN} and V_{WN} from an extrapolation using the values at $(m-2)\,\Delta t$ and $(m-3)\,\Delta t$ on $x = L$. The rest of the procedure is the same as above.

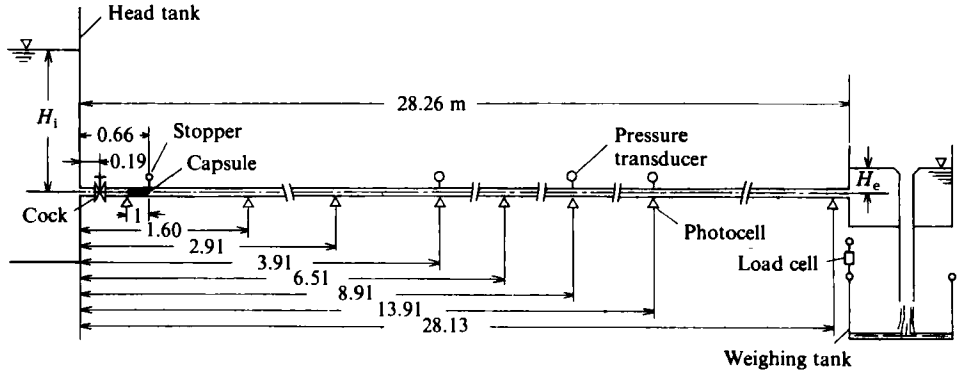

FIGURE 6. Experimental set-up.

No.	d (mm)	l (mm)	M (kg)	$\frac{M-\rho Vc}{M}$	ζ
1	36	198	0.210	0.0420	0.423
2	36	198	0.625	0.6781	0.423
3	38	209	0.240	0.0142	0.452
4	38	209	0.647	0.6343	0.452

TABLE 1. Specification of capsules used

4. Experiment and numerical data for computation

Figure 6 shows the experimental set-up. The pipeline, made of transparent acrylic tubes, was of length 28.26 m, inside diameter 40 mm and outside diameter 48 mm. The experiment was carried out under the condition of constant inlet and exit heads. The inlet head ranged from 0.94 to 2.34 m, while the exit head was maintained at 0.12 m. The flow rate was measured by weighing the fluid at the pipe exit. The pressure was measured at three points in the pipeline by pressure transducers. We monitored the motion of the capsule by using eight photocells placed on the pipeline. Table 1 shows the specifications of the capsules, which are drawn in figure 7. These capsules have eight wheels to keep their posture coaxial with the pipe.

The experiments began by manually opening the cock near the pipe inlet, which took about 1.3 s to fully open. This cock handling was simulated in the computation. The propagation speed of the pressure wave was experimentally determined as 554.2 m/s because we could not obtain the Young's modulus of the pipe material. The inferred modulus from this value is 3.556×10^9 Pa, which is a reasonable value compared with those of similar plastics. The coefficient of Coulomb friction was determined to be 0.02, the loss coefficient of the pipe inlet was 0.56, and that of the cock was 0.51 when fully opened. The step in the axial direction Δx was 0.01 L and that in time Δt was $\Delta x/4a$. The validity of using this grid system was confirmed by comparing the analytical solution for steady water flow with this computation.

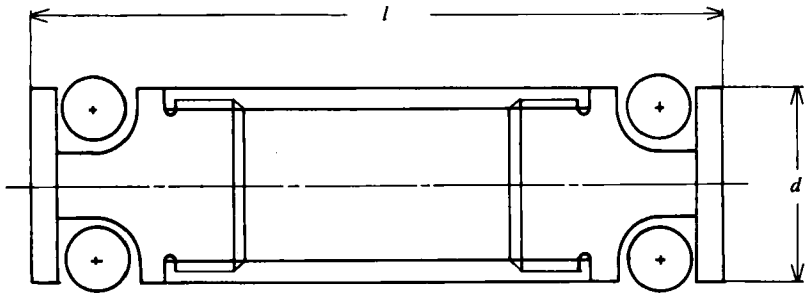

FIGURE 7. Wheeled capsule.

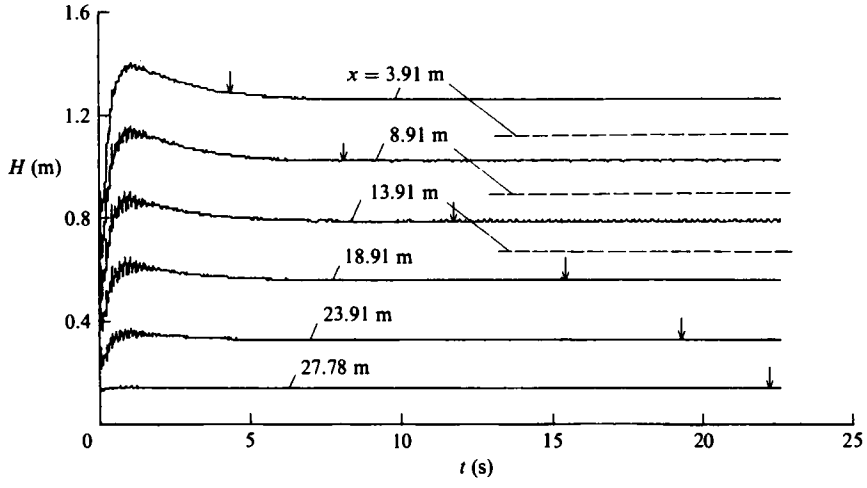

FIGURE 8. Time histories of pressures at several points in the pipeline for capsule 1 at $H_i = 1.56$ m: ---- experiment; ——, computation.

5. Results and discussion

Figure 8 shows time histories of pressures at several points in the pipeline for capsule 1 where H_i is the inlet head. The dashed lines show steady-state values of pressure from the experiment and the arrows show the time when the capsule passes the point. It is difficult to detect when the capsule passes from the time histories of pressure alone. In a pneumatic capsule pipeline there is a sharp pressure rise when capsule passes, see Tomita, Abe & Jotaki (1981). This shows that the pressure drop caused by the capsule is very small, and this is in part caused by its small solid friction. The computation proves that the pressure drop $p_R - p_F$ of the capsule with a large diameter is at most 7 mm of water at the capsule's final velocity. The discrepancy between measurement and computation is thought to be due to incomplete head control in the experiment.

Figure 9 shows time histories of water velocity at the pipe exit and the velocity of capsule 2. The capsule attains a constant speed in a short time. The water velocity is higher than the capsule velocity just after the opening of the cock, but is soon outstripped by the capsule. The computation showed that the water velocities at various points along the pipeline are almost the same for a given time. The velocity histories for other stations are almost the same as shown in figure 9.

Figure 10 shows trajectories of capsule 4 for different inlet heads. It is found that

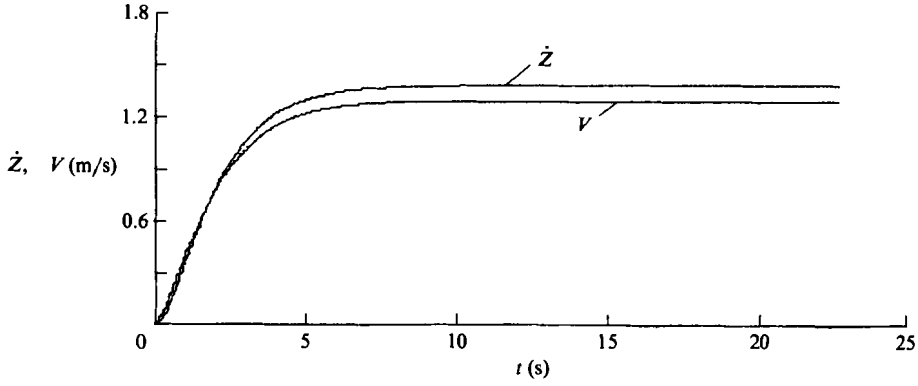

FIGURE 9. Time histories of capsule and water velocities for capsule 2 at $H_1 = 1.56$ m; computation.

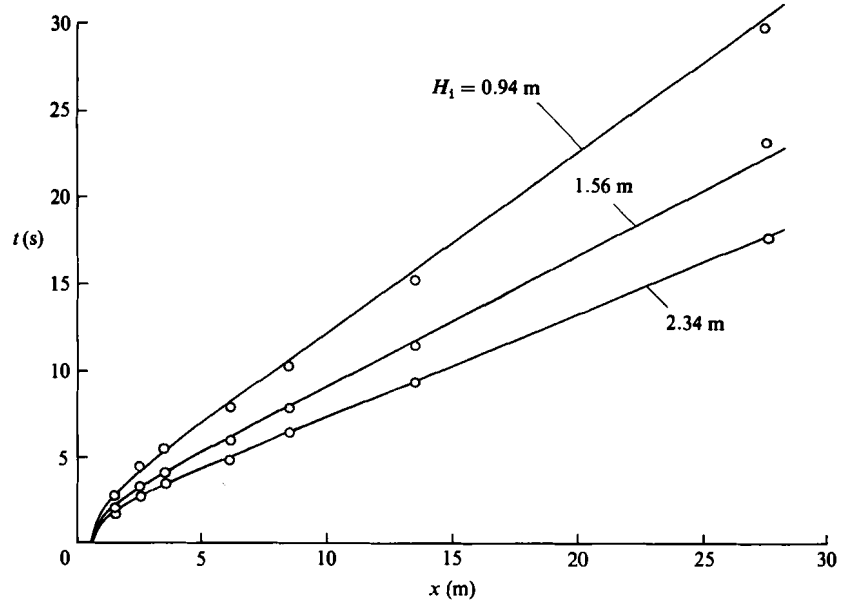

FIGURE 10. Trajectories of capsule 4: ○, experiment; ——, computation.

for a given head the capsule motion is not dependent on the mass and length of the capsule but on the diameter. As a result of the computation, figure 11 shows $\dot{Z}_s/V_s$ against V_s, where $\dot{Z}_s$ and V_s are the final velocities of the capsule and the water at the pipe exit. The computation was done for four inlet heads: 0.30, 0.94, 1.56 and 2.34 m. Similar results were obtained by Ellis (1964) for capsules with density equal to that of the water. Figure 12 shows $\dot{Z}_s$ and V_s, $\dot{Z}_s$ being always higher than V_s both in the experiment and the computation. The three groups of data in figure 12 are experimental results from the heads of 0.94, 1.56 and 2.34 m.

We now discuss the forces acting on the capsule which are derived from the computation. They are the pressure, shear and Coulomb friction forces. We consider them as a form of acceleration. We denote A_p as F_p/M, A_s as F_s/M and A as a total acceleration. Then, $A_p + A_s - A$ is due to the Coulomb friction. Figures 13, 14 and

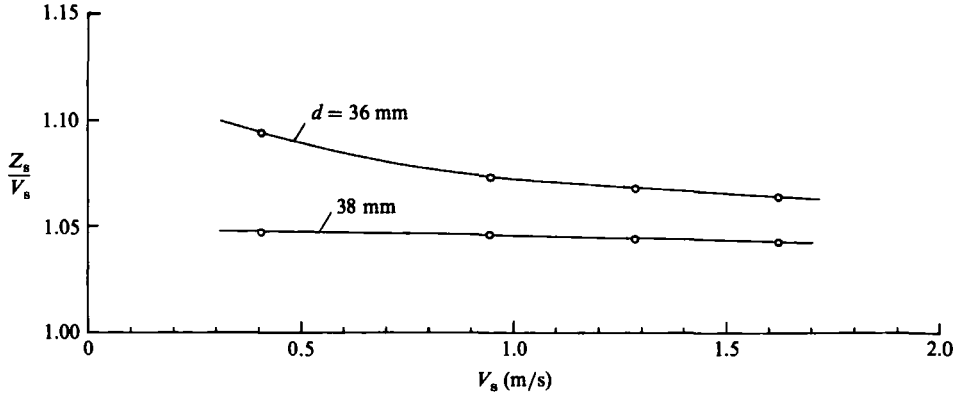

FIGURE 11. Velocity ratio of a capsule at the final state: ○, computation.

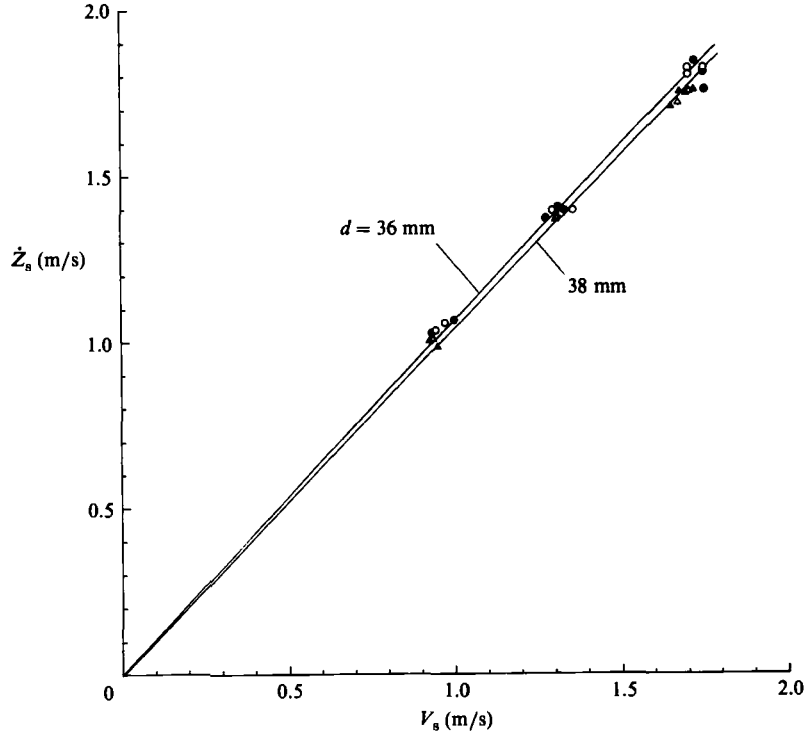

FIGURE 12. Capsule and water velocities at the final state: ○, capsule 1; ●, capsule 2; △, capsule 3; ▲, capsule 4; ——, computation.

15 show time histories of A, A_p and A_s. Figure 13 shows capsule 2 at $H_1 = 1.56$ m, where both F_p and F_s are driving forces that decrease as the final state is reached. Figure 14 shows capsule 1 at $H_1 = 2.34$ m, where the driving force in the final state is the shear force, and the pressure force becomes the resistance. However, in this case p_R is larger than p_F. Figure 15 shows capsule 3 at $H_1 = 1.56$ m, where the pressure force is the driving force and the shear force is the resistance.

Figure 16 shows A_p and A_s at the capsule's final speed before leaving the tube. When the capsule diameter is large, the pressure force is the driving force while the shear force is the resistance. On the other hand, when the capsule diameter is small

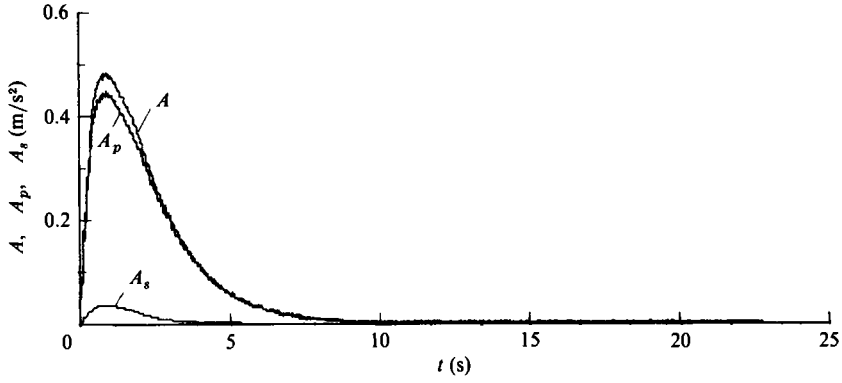

FIGURE 13. Time histories of acceleration due to pressure and shear forces by capsule 2 at $H_1 = 1.56$ m; computation.

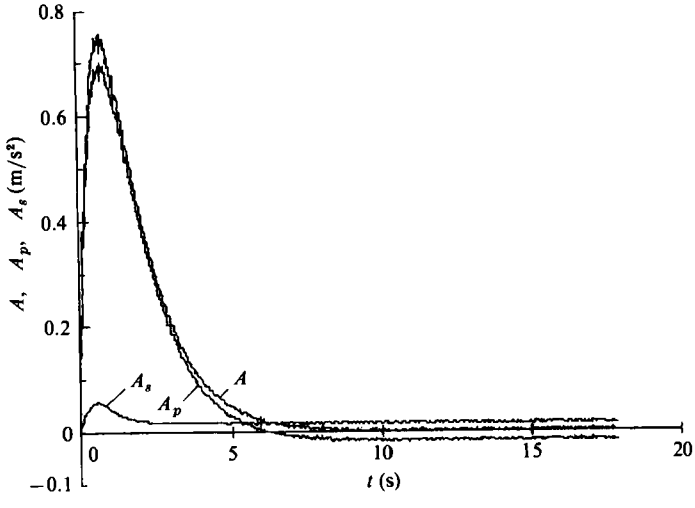

FIGURE 14. Time histories of acceleration due to pressure and shear forces of capsule 1 at $H_1 = 2.34$ m; computation.

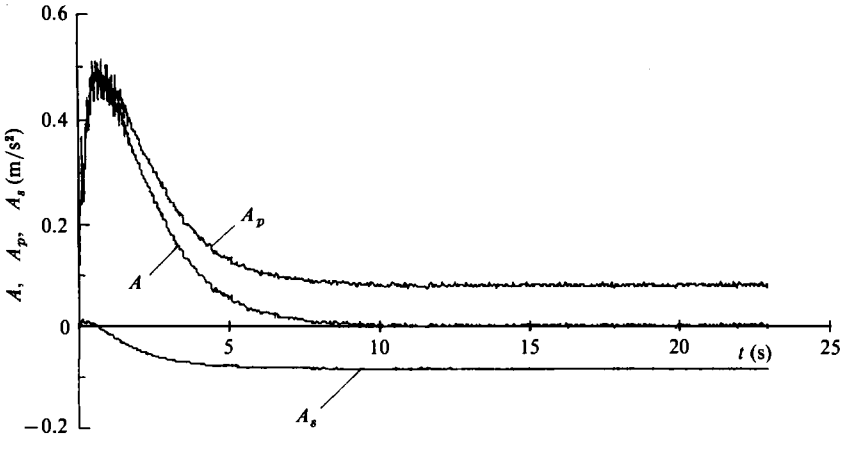

FIGURE 15. Time histories of acceleration due to pressure and shear forces of capsule 3 at $H_1 = 1.56$ m; computation.

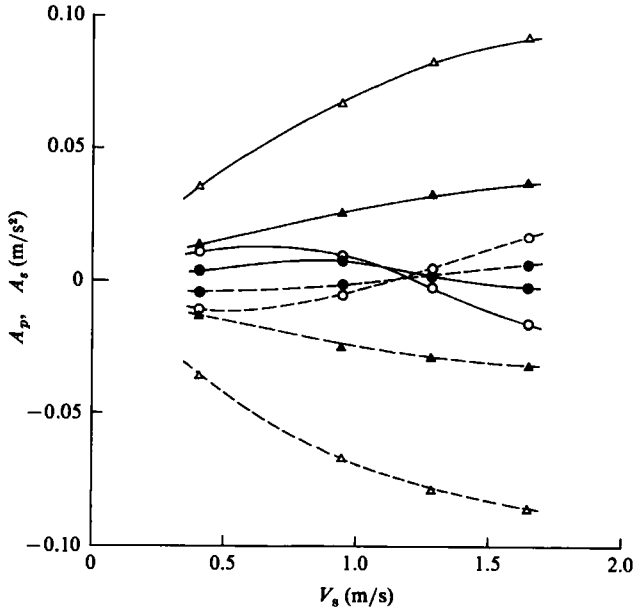

FIGURE 16. Acceleration and water velocity at the final state by computation: ○, capsule 1; ●, capsule 2; △, capsule 3; ▲, capsule 4; ——, due to pressure force; – – – –, due to shear force.

and the water velocity is high, the shear force becomes the driving force. Even with the same diameter, the magnitude of A_p and A_s for light capsules is higher than that for heavy capsules. However, F_p and F_s for both capsules have the same order of magnitude.

6. Conclusion

This work could become a basis for the analysis of a hydraulic capsule transport system. For example, it would be possible to extend the present method of computation to the case where capsules are continuously fed into a pipeline. It is important to monitor the motion of individual capsules in the pipeline because there is sometimes a problem in handling capsules at the destination due to the random arrival in spite of the regular departure. It is important to apply an appropriate flow model around the capsule to give an accurate prediction of capsule motion. This is also a problem with non-wheeled capsules which will be widely used in practice.

We would like to thank Mr H. Nakamura for his cooperation with this work.

REFERENCES

ELLIS, H. S. 1964 *Can. J. Chem. Engng* **42**, 1.

LIU, H. 1981 *J. Pipelines* **1**, 11.

LUR'E, M. V. & GOL'DZBERG, V. L. 1971 *Izv. Akad. Nauk SSSR, Energetika i Transport* **4**, 99 (in Russian).

POLDERMAN, H. G. 1982 *J. Pipelines* **3**, 123.

TOMITA, Y., ABE, K. & JOTAKI, T. 1981 *Bull. JSME* **24**, 1579.

TSUJI, Y., MORIKAWA, Y. & CHONO, S. 1980 Pneumotransport 5. *BHRA Fluid Engineering Paper* G2.

YANAIDA, K. 1980 *J. Mining & Metall. Inst. Japan* **96**, 80 (in Japanese).

YOKOGAWA, A., SUZUKI, M., ISAKA, M., TACHIBANA, T. & YAMAMOTO, K. 1980 *Hitachi Zosen Giho* **41**, 54 (in Japanese).

ZUCROW, M. J. & HOFFMAN, J. D. 1976 *Gas Dynamics*, vol. 1. Wiley.